Lithos 360–361 (2020) 105449

Contents lists available at ScienceDirect

Lithos

journal homepage: www.elsevier.com/locate/lithos

Research Article

Geology and geochronology of the super-large Bailongshan Li–Rb–(Be) rare-metal pegmatite deposit, West Kunlun orogenic belt, NW China

He Wang [a], Hao Gao [a,b], Xiao-Yu Zhang [a,b], Qing-He Yan [a,c,*], Yigang Xu [c], Kailin Zhou [a,b], Rui Dong [a,b], Pei Li [a,b]

[a] CAS Key Laboratory of Mineralogy and Metallogeny, Guangzhou Institute of Geochemistry, Chinese Academy of Sciences, Guangzhou 510640, China
[b] University of Chinese Academy of Sciences, Beijing 100049, China
[c] State Key Laboratory of Isotope Geochemistry, Guangzhou Institute of Geochemistry, Chinese Academy of Sciences, Guangzhou 510640, China

ARTICLE INFO

Article history:
Received 30 May 2019
Received in revised form 18 February 2020
Accepted 24 February 2020
Available online 29 February 2020

Keywords:
Bailongshan rare-metal pegmatite deposit
Coltan and zircon U
Pb age
Regional and internal zonation
West Kunlun
Songpan
Garzê rare-metal pegmatite metallogenic belt

ABSTRACT

The Bailongshan pegmatite deposit is a newly discovered super-large Li–Rb–(Be–Ta–Nb) rare-metal deposit in the West Kunlun orogenic belt, northwest China. Fifty-two rare-metal orebodies (50–1230 m long by 1.5–157 m wide) have been discovered by detailed field surveying, making up a metallogenic field that is larger than 8250 × 400 m. The deposit is estimated to have ore reserves of more than 5.06 million tonnes (t) Li_2O, 160,020 t BeO, 316,200 t Rb_2O, 40,060 t Nb_2O_5, and 10,750 t Ta_2O_5. Pegmatite dikes are zoned around a granodiorite batholith, ranging from barren through orebodies rich in Be, Nb, Ta, Rb, and Li with increasing distance from the batholith, similar to the classical model of a zoned Li–Ce–Ta (LCT)-type pegmatite. LA–ICP–MS analyses of coltan and zircon yield $^{206}Pb/^{238}U$ ages of 208.1 Ma and 212.3 Ma, respectively, representing the emplacement ages of the pegmatites and granodiorite. These data indicate a temporal link between the emplacement of the granodiorite batholith and rare-metal mineralization in the pegmatites, and that the Bailongshan rare-metal pegmatites are temporospatially related to the granodiorite batholith. The Bailongshan pegmatites and other rare-metal pegmatite deposits in the West Kunlun orogenic belt likely make up a >600-km-long Li metallogenic belt, and further exploration for rare-metal pegmatites should be focused on the area adjacent to Late Triassic granitoid plutons in the belt. This belt likely extends to the East Kunlun and West Sichuan rare-metal belts, forming the >2000-km-long, Late Triassic West Kunlun–Songpan–Garzê rare-metal metallogenic belt.

1. Introduction

Granites, pegmatites, and salt-lake brines are major hosts of lithium (Li), with Li resources in China being hosted mainly in salt-lake brines, with limited granite, and pegmatite ore reserves (Li et al., 2015). However, it is easier to extract Li from granites and pegmatites than from salt-lake brines due to the high Mg/Li ratios of the latter (Yang et al., 2012). Previous exploration in China has discovered Li-bearing granites and pegmatites in the Altai, South China, West Sichuan, and West Kunlun Li metallogenic belts (Li et al., 2015). The Altai metallogenic belt contains more than 35 pegmatite ore fields including the Koktokay, Kelumute, Kukalagai, Kalu'an–Azubai, and Askaerte pegmatite deposits, formed during the Caledonian, Hercynian, Indosinian, and Yanshanian orogenies. The major ore-forming stage occurred in the Indosinian orogeny, and was closely related to the evolution of the Paleo-Asian ocean (Li et al., 2015). The South China metallogenic belt hosts several giant granite- and pegmatite-hosted rare-metal (Li, Rb, Cs, Ta, W, and Sn) deposits, including the Yichuan, Jianfengling, and Zhengchong deposits formed in the Caledonian, Indosinian, and Yanshanian, respectively. The major ore-forming stage was in the Yanshanian and was closely related to subduction of the Paleo-Pacific Plate beneath the southeastern China continental margin (Li et al., 2015). The West Sichuan metallogenic belt includes the Jiajika super-large deposit, the Ke'eryin large deposit, and four medium-sized deposits (Li et al., 2015). These deposits formed in the Late Triassic to Early Cretaceous, closely related to the evolution of the Paleo-Tethys Ocean (Li et al., 2019).

Pegmatites are widely distributed along the West Kunlun orogenic belt, an economically important rare-metal metallogenic belt (Yan et al., 2018; Zhou et al., 2011). However, previous exploration surveys discovered only one medium and a few small rare-metal pegmatite deposits in this belt before the Bailongshan Li–Rb–(Be) rare-metal pegmatite deposit was discovered in 2017 (Wang et al., 2017). An initial evaluation shows that it is a super-large Li–Rb–(Be) rare-metal deposit, with ore reserves of 3.45 Mtonne (Mt) Li_2O and 176,000 t Rb_2O (Wang et al., 2017). More pegmatite orebodies have been discovered in the past two years but several crucial questions about the deposit remain, concerning (1) when the ore was formed; (2) the relationship between Li–Rb–(Be) mineralization and the evolution of the pegmatites; and

* Corresponding author at: CAS Key Laboratory of Mineralogy and Metallogeny, Guangzhou Institute of Geochemistry, Chinese Academy of Sciences, Guangzhou 510640, China.
E-mail address: yanqinghe@gig.ac.cn (Q.-H. Yan).

https://doi.org/10.1016/j.lithos.2020.105449
0024-4937/

(3) the relationship between the abundant pegmatite dikes and the adjacent granitoid batholith.

Here we describe the regional and internal zonation of the pegmatite dikes, and provide new laser ablation–inductively coupled plasma–mass spectrometry (LA–ICP–MS) coltan and zircon U—Pb ages for the rare-metal pegmatite dike and adjacent granodiorite batholith. These data allow us to constrain the origin of the deposit and the relationship between Li–Rb–(Be) mineralization and the evolution of the pegmatites, which may be useful for further exploration for rare-metal deposits in the West Kunlun metallogenic belt.

2. Regional geology

The West Kunlun orogenic belt is bordered by the Tibetan Plateau to the south and Tarim Basin to the north (Fig. 1a; Hu et al., 2016), and comprises four terranes accreted during subduction of the Proto- and Paleo-Tethys oceans: the North Kunlun, South Kunlun, Tianshuihai, and Karakorum–Qiangtang terranes (from north to south; Mattern and Schneider, 2000; Xiao et al., 2002a, b, 2003a, b). These terranes are separated by the Oytag–Kudi, Mazar–Kangxiwar, and Konggashankou–Qogir sutures, respectively (Fig. 1a; Deng, 1995; Yin and Bian, 1995; Ding et al., 1996; Matte et al., 1996; Pan, 1996; Mattern and Schneider, 2000).

The Tianshuihai terrane trends northwest–southeast and is bounded by the Mazar–Kangxiwar suture to the north and the Hongshanhu–Qianertianshan suture to the south (Fig. 1b). The terrane comprises Precambrian basement and overlying Phanerozoic strata. The Precambrian basement comprises the Tianshuihai, Bulunkuole, and Saitula groups (Fig. 1b). The Tianshuihai Group comprises a suite of greenschist-facies, shallow-marine siliciclastic rocks and limestone (Fig. 1b; Hu et al., 2016). The Tianshuihu Formation comprises mainly gray-black carbonaceous slate, carbonaceous siltstone, and fine-grained dolomite-bearing limestone. The lower Silurian Wenquangou Formation comprises thick layers of gray-green to light-gray feldspar–quartz sandstone. The Tianshuihai terrane is thought to have been an accretionary prism during the Paleozoic–Mesozoic, and contains thick, partly metamorphosed Triassic flysch sequences that record subduction-related orogenic process from the collision between the South Kunlun and Karakorum–Qiangtang terranes (e.g., Matte et al., 1996; Mattern and Schneider, 2000; Yin and Harrison, 2000; Xiao et al., 2002a, 2003a, 2005).

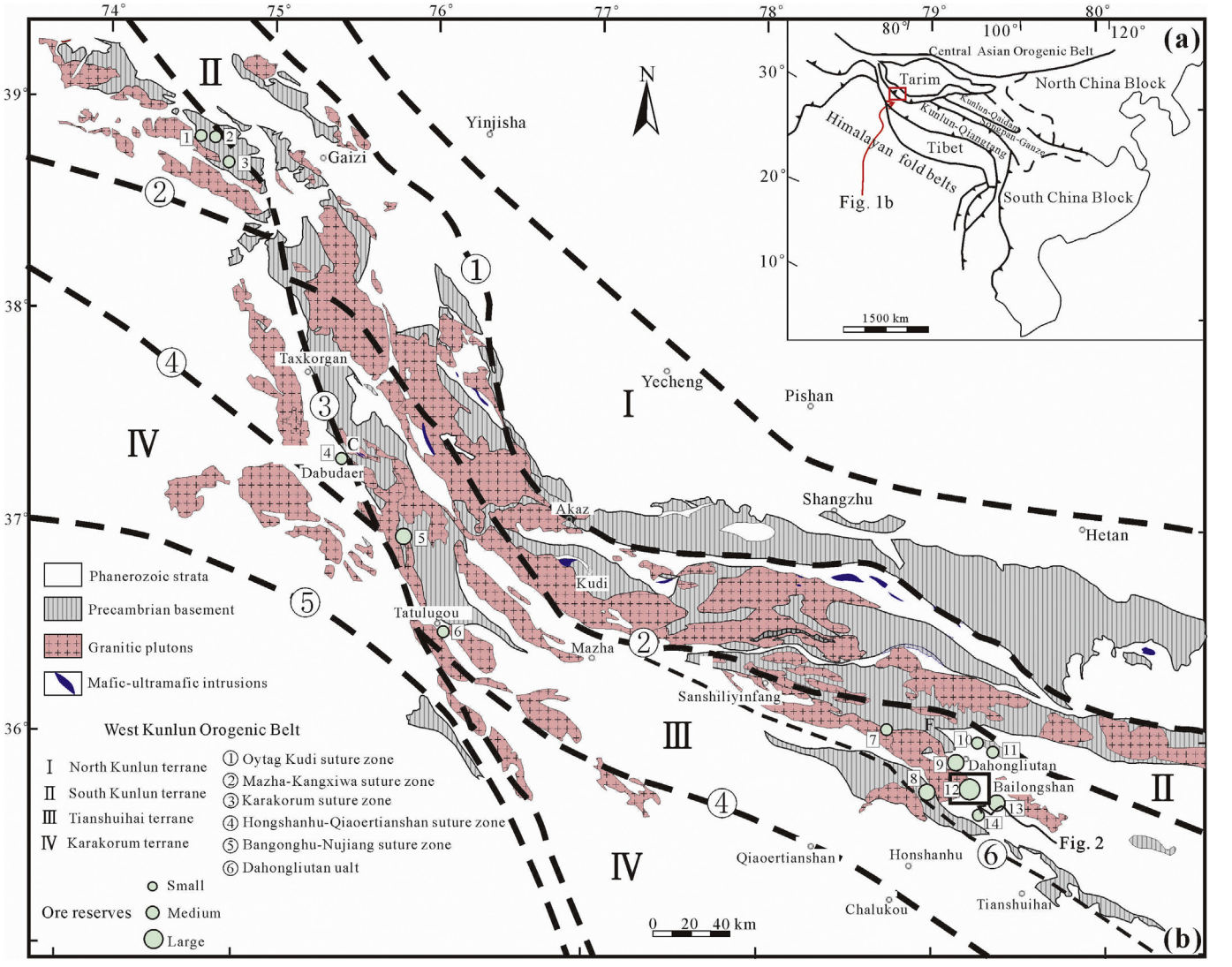

Fig. 1. (a) Regional map (after Pan et al., 2004; Xiao et al., 2005) and (b) simplified geological map of the West Kunlun orogenic belt, Xinjiang, northwest China (after Huang, 2014; Yan et al., 2018). The light green dots denote the main rare-metal pegmatite deposits of the West Kunlun orogenic belt. 1 Kalawala; 2 Xiaoerbulong; 3 Hushitashi; 4 Dabudaer; 5 Sansu; 6 Tatulugou; 7 Kangxiwa; 8 Zhongfulugou; 9 Dahongliutan; 10 No. 496; 11 Akeshayi; 12 Bailongshan; 13 Xufengling; 14 Bingzhou. Small deposits contain <10,000 t, medium deposits <100,000 t, and large deposits >100,000 t Li_2O.

Granitoid plutons and pegmatites are widely distributed along the Mazar–Kangxiwar suture (Fig. 1b). Fourteen rare-metal deposits have been discovered in the pegmatites, including the Huoshikashi, Kalawala, Xiaoerbulong, Dabudaer, Sansu, Tatulugou, Kangxiwa, Zhongfulugou, No. 496, Akeshayi, Dahongliutan, Bailongshan, Xufengling, and Bingzhou deposits, forming the 600-km-long West Kunlun rare-metal belt (Fig. 1b; Wang et al., 2017; Yan et al., 2018). The deposits are distributed mainly within three regions along the belt: Muji–Bulunkou, Dabudaer–Tatulugou, and Dahongliutan–Bailongshan (from northwest to southeast). More than 7000 pegmatites have been found in the Dahongliutan–Bailongshan region, striking to the northwest, 0.5–157 m wide by 2–1230 m long, and hosted mainly in either the metamorphic rocks of the Bayan Har Mountain Group or in granite plutons (Fig. 2; Zhou et al., 2011; Yan et al., 2018). Previous exploration in this region discovered the Bailongshan super-large rare-metal deposit (Wang et al., 2017), the Xuefengling large rare-metal deposit (Wang et al., 2019) and the Dahongliutan medium-sized rare-metal deposit (Yan et al., 2018).

3. Bailongshan Li–Rb–(Be) rare-metal pegmatites

The Bailongshan Li–Rb–(Be) rare-metal pegmatites are characterized by Li, Rb, Be, Nb, Ta, and Sn mineralization, and belong to the LCT family in the classification proposed by Černý and Erict (2005). The country rocks comprise quartz sandstone, sericite–quartz schist, and two-mica schist of the Late Triassic Bayan Har Mountain Group, which strikes 110°–150° and dips NE at 45°–80°. The Bailongshan pegmatites abut the regional WNW-striking Dahongliutan fault to the southwest (Fig. 1b), and are close to the Bailongshan granodiorite batholith to the northwest (Figs. 1b, 2, 3a), and a few small two-mica and muscovite granite plutons to the southeast (Figs. 2, 3c–d). Of the hundreds of pegmatites that crop out in the region, only 47 host economic Li mineralization and only 5 host Be mineralization. Most barren pegmatites are close to the granodiorite batholith and granitic plutons, while the Li- and Be-rich pegmatites are generally more distant (Fig. 2).

The Li- and Be-rich pegmatites constitute a NW-striking > (8250 × 400)-m metallogenic field dipping at 65°–90°. Individual

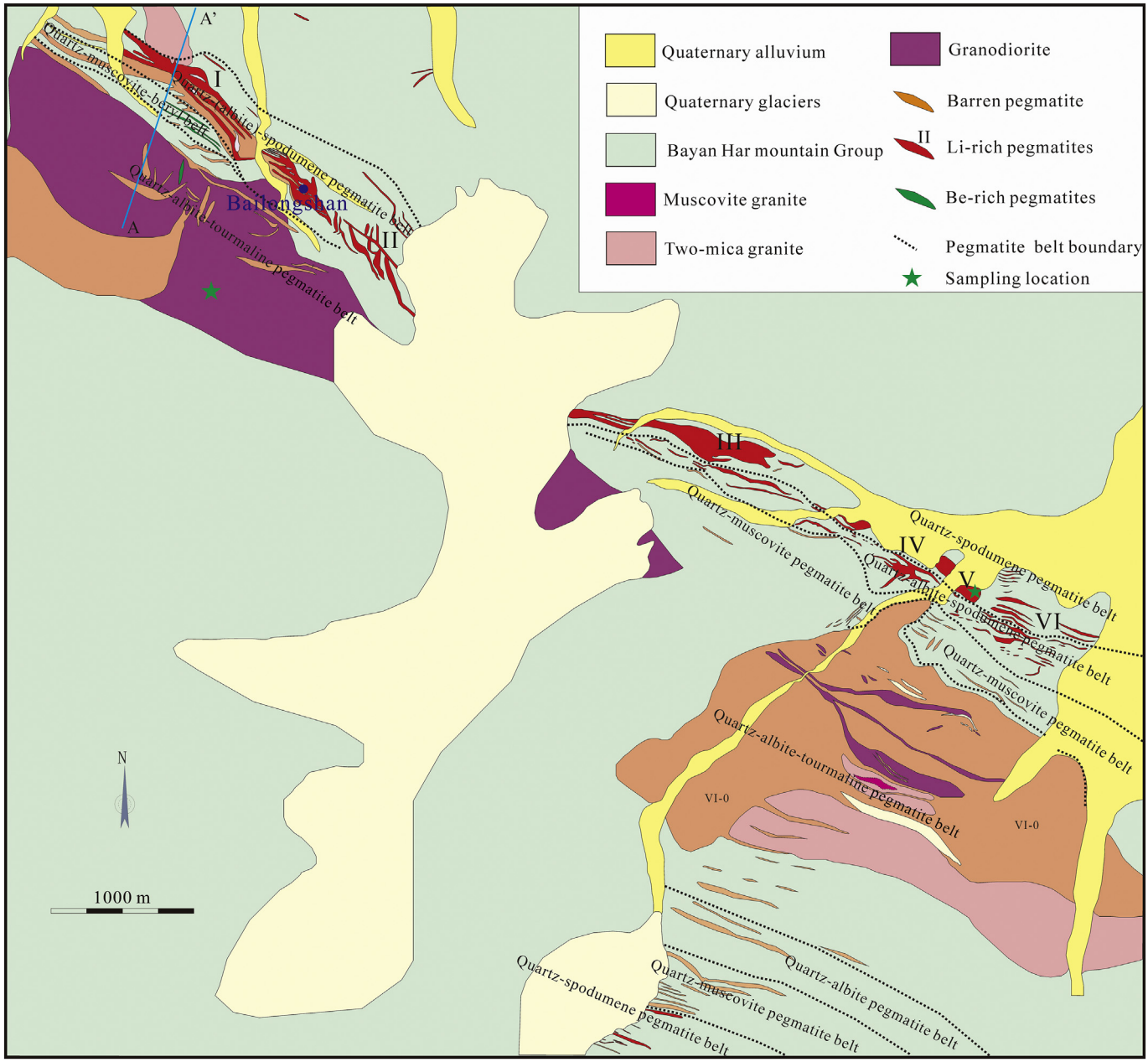

Fig. 2. Simplified geological map of the Bailongshan region.

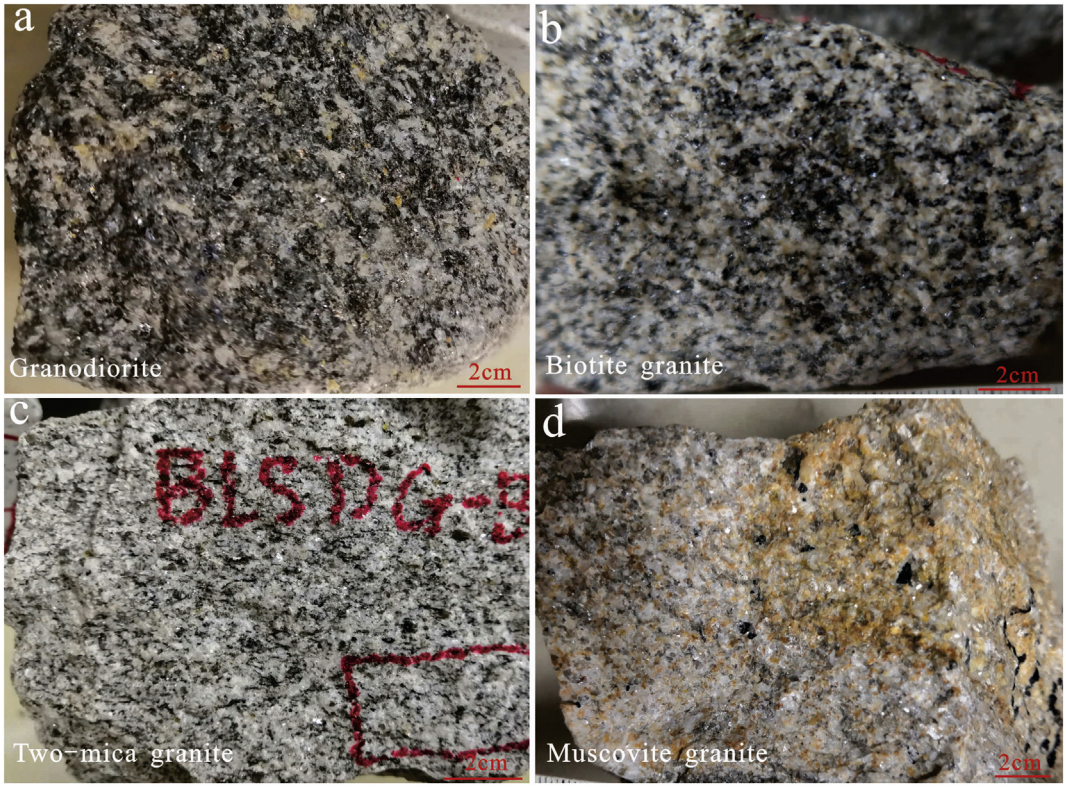

Fig. 3. Photographs of representative granitoid samples.

pegmatite dikes are usually lens-like, and are 1.5–157 m wide by 50–1230 m long (Fig. 2). The metallogenic field is divided into six segments (I–VI) from northwest to southeast based on the occurrence of pegmatite dikes (Fig. 2). There 52 orebodies: 3 Li-rich orebodies in Segment I, 10 in Segment II, 12 in Segment III, 4 in segment IV, 3 in Segment V, and 15 in Segment VI, as well as 5 Be-rich orebodies in Segment I. Deposit sizes and ore grades are listed in Table 1.

The estimated ore reserves of the Bailongshan pegmatites are 5.06 Mt. Li_2O, 160,020 t BeO, 316,200 t Rb_2O, 40,060 t Nb_2O_5, and 10,750 t Ta_2O_5. The two largest orebodies in the deposit are numbered II-1 and III-2. Orebody II-1 is 116 m long by 81–152 m wide; orebody III-2 is 990 m long by 60–152 m wide (Fig. 4); together they contain ~49% of the Li_2O, ~56% of the BeO, and ~66% of the Rb_2O in the Bailongshan rare-metal deposit.

3.1. Regional zonation

Well developed regional zonation is observed in the pegmatites of segments I and VI. The pegmatites are zoned from barren to rare-metal-rich with increasing distance from the Bailongshan granodiorite plutons (Figs. 2, 5, 6). The barren pegmatites in Segment VI are roughly symmetric around the two-mica granite, with the Li-rich pegmatites being in the farthest belt (Fig. 2). In Segment VI there is, with increasing distance to the north of the two-mica granite, a wide quartz–albite–tourmaline belt (Figs. 2, 7e–h), a quartz–muscovite pegmatite belt (Figs. 2, 7c), a quartz–albite–spodumene pegmatite belt (Figs. 2, 7b), and a quartz–spodumene pegmatite belt (Figs. 2, 7a). Our field investigation demonstrates that the pegmatites to the south of the two-mica granite mirror this distribution (Fig. 2), consistent with the classical model of a zoned LCT-type pegmatite field (Černý, 1989).

Segment I comprises mainly the least-evolved barren pegmatites with a similar regional zonation to Segment VI. From south to north, quartz–albite–tourmaline pegmatites intrude the granodiorite batholith; there is a Be-rich quartz–muscovite–beryl pegmatite belt, and a Li-rich quartz–(albite)–spodumene pegmatite belt (Fig. 2).

3.2. Internal zonation

Orebodies I-1 and II-1 are zoned in terms of their mineral assemblages, grain sizes, and textures. The I-1 Li-rich orebody is located in the quartz–(albite)–spodumene belt, and is >280 m wide. Five internal zones were identified in it: an elbaite–albite–muscovite zone, a blocky albite–quartz zone, a quartz–muscovite zone, a quartz–albite–spodumene zone, and a quartz–spodumene zone (from south to north; Figs. 5a, 6). A quartz–muscovite zone occurs locally within the quartz–spodumene zone (Fig. 5a). The II-1 Li-rich orebody is >115 m wide with three internal zones: a blocky albite–quartz zone, a quartz–albite–spodumene zone, and a quartz–spodumene zone (from south to north; Fig. 5b).

The barren pegmatites in Segment VI (VI-0) are >1000 m wide and eight zones have been identified in the field: from center to rim, a quartz–muscovite zone (Fig. 7d), a layered aplite (quartz–tourmaline–muscovite) zone (Fig. 7e), a medium-sized quartz–tourmaline–muscovite zone, a blocky albite–quartz–tourmaline zone (Fig. 7f), a fine- to medium-grain quartz–albite–tourmaline zone (Fig. 7g), a graphic zone (Fig. 7h), an aplite zone, and an interlayer pegmatite (layered aplite).

4. Sample descriptions and analytical methods

4.1. Sample descriptions

The location of the granodiorite sample (BLS–b5) collected for zircon U—Pb dating is shown in Fig. 2. The granodiorite is fine-grained and comprises 5–10 vol% amphibole, 10–20 vol% biotite, 15%–18 vol% quartz, and 50–60 vol% feldspar (Fig. 3a).

Samples for coltan U—Pb geochronology were collected from the quartz–spodumene pegmatite belt in the center of orebody V-1

Table 1
Grades of LiO_2, BeO, Rb_2O, Cs_2O, Nb_2O_5, and Ta_2O_5 of the main ore body in the Bailongshan Li-Rb-(Be) deposit.

Ore block	Orebody No.	Length (m)	Width (m)	Li_2O (wt%)	BeO (wt%)	Rb_2O (wt%)	Cs_2O (wt%)	Nb_2O_5 (wt%)	Ta_2O_5 (wt%)	Reference
I	I -1	1230	61.86	1.26	0.055	0.1	0.005	0.011	0.003	
	I -2	210	3.1	1.53	0.062	0.079	0.005	0.02	0.02	
	I -3	120	1.8	2.21	0.04	0.088	0.009	0.005	0.002	
	I -4	390	9.66	0.008	0.097	0.067	0.003	0.012	0.002	
	I -5	410	5.64	0.03	0.06	0.033	0.004	0.023	0.003	
	I -6	230	1.88	0.05	0.055	0.032	0.004	0.009	0.001	
	I -7	310	3.76	0.045	0.082	0.057	0.007	0.007	0.001	
	I-8	180	9.37	0.045	0.45	0.049	0.002	0.016	0.002	
II	II -1	730	115.85	1.47	0.057	0.12	0.012	0.013	0.006	
	II -2	160	11.56	1.96	0.042	0.091	0.008	0.012	0.006	
	II -3	290	3.85	1.68	0.074	0.034	0.004	0.009	0.002	
	II -4	450	34.67	1.83	0.055	0.054	0.005	0.013	0.004	
	II -5	520	7.7	2.77	0.046	0.077	0.017	0.031	0.015	
	II -6	320	26.96	2.07	0.071	0.066	0.015	0.017	0.01	
	II -7	490	19.26	2.48	0.048	0.112	0.012	0.01	0.006	
	II -8	590	5.8	3.06	0.011	0.036	0.006	0.006	0.004	
	II -9	170	2.2	5.47	0.007	0.057	0.009	0.008	0.011	
	II-10	170	2.2	1.99	0.052	0.069	0.006	0.015	0.009	
III	III -1	420	23.5	1.52	0.012	0.039	0.003	0.028	0.01	
	III -2	990	97.96	1.6	0.054	0.139	0.009	0.014	0.007	
	III -3	150	9	2.56	0.01	0.093	0.033	0.014	0.007	
	III -4	660	9.5	3.4	0.017	0.039	0.006	0.009	0.007	
	III -5	480	5	2.54	0.045	0.13	0.01	0.01	0.02	
	III -6	140	9.3	2.26	0.037	0.19	0.018	0.019	0.006	
	III -7	220	5	1.13	0.079	0.028	0.004	0.07	0.05	
	III -8	160	3.2	2.33	0.047	0.052	0.004	0.019	0.006	
	III -9	110	2.8	3.44	0.029	0.026	0.002	0.017	0.008	
	III -10	75	5.5	2.1	0.079	0.027	0.003	0.056	0.019	
	III -11	100	3							
	III-12	90	2							
IV	IV-1	530	45.52	2.17	0.054	0.092	0.01	0.014	0.007	
	IV-2	290	26.8	1.66	0.046	0.028	0.009	0.011	0.002	
	IV-3	310	5.6	2.78	0.056	0.046	0.002	0.028	0.008	
V	V-1	390	93.03	1.88	0.063	0.153	0.02	0.015	0.009	
	V-2	65	8.3	1.96	0.042	0.091	0.008	0.012	0.006	
	V-3	175	5.5	1.78	0.059	0.11	0.011	0.013	0.007	
VI	VI -1	339	25.8	1.93	0.04	0.11	0.01	0.016	0.006	
	VI -2	369	13.51	1.85	0.027	0.045	0.008	0.014	0.002	
	VI -3	708	5.17	2.81	0.044	0.079	0.009	0.009	0.003	
	VI -4	673	7.1	1.61	0.063	0.079	0.012	0.017	0.012	
	VI -5	702	13.44	2.31	0.055	0.11	0.009	0.018	0.008	
	VI -6	360	5.6	1.74						
	VI -7	447	2.11	1.5						
	VI -8	357	14.08	0.93						Peng et al., 2018
	VI -9	270	4.61	2.05						
	VI -10	323	4.72	2.15						
	VI-11	180	4.04	3.44			0.011	0.008	0.005	
	VI -12	140	2.15	0.73						
	VI -13	120	3							
	VI -14	170	8.75	2.57						
	VI -15	150	5							

(Fig. 8a). The samples contain feldspar (5–10 vol%), quartz (40–50 vol %), spodumene (40–45 vol%), black tourmaline (2 vol%), light-green elbaite (2 vol%), muscovite (2 vol%), montebrasite (1 vol%), coltan (1 vol%) and trace amounts of cassiterite (Fig. 8a, b). Quartz crystals are 0.4–3 cm long, and spodumene megacrysts are 3–30 cm long (Fig. 8a). Coltan is commonly intergrown with spodumene and quartz (Fig. 8b). The coltan crystals exhibit oscillatory and sector zoning (Fig. 8c, d), similar to typical magmatic coltan (Linnen and Cuney, 2005).

Zircon and coltan crystals were separated from rocks using conventional heavy-liquid and magnetic methods, then handpicked under a binocular microscope, mounted in epoxy resin, and polished. Prior to LA–ICP–MS analysis, cathodoluminescence (CL) images of zircons were acquired using a JXA-8100 electron-probe microanalyzer (EPMA) with a Mono CL3 CL system at the Guangzhou Institution of Geochemistry, Chinese Academic of Sciences (GIGCAS), Guangzhou, China. Back-scattered-electron (BSE) images of coltan were obtained using a JEOL JXA-8230 EPMA at the CAS Key Laboratory of Mineralogy and Metallogeny, GIGCAS. The CL and BSE images ensured that the analyzed zircon and coltan crystals were fresh and lacked inclusions and cracks.

4.2. LA–ICP–MS zircon U—Pb dating

LA–ICP–MS zircon U—Pb dating was carried out using an Agilent 7500a ICP–MS coupled to a 193-nm wave laser microprobe at the Key Laboratory of Mineralogy and Metallogeny, GIGCAS. A laser energy of 80 mJ, frequency of 10 Hz, ablation period of 40 s, and a spot diameter of 31 μm were used. U, Th, and Pb concentrations were calibrated using ^{29}Si as an internal standard, and US National Institute of Technology and Standards (NIST) 610 glass as the reference standard. A Temora standard zircon was used for age calibration ($^{206}Pb/^{238}U$ age 416.8 Ma; Black et al., 2003), and a 91,500 zircon was analyzed once every five analyses as an external standard. Analytical procedures have been described earlier by Li et al. (2011). Data reduction was performed offline using ICPMSDataCal software (Liu et al., 2010). Common-Pb

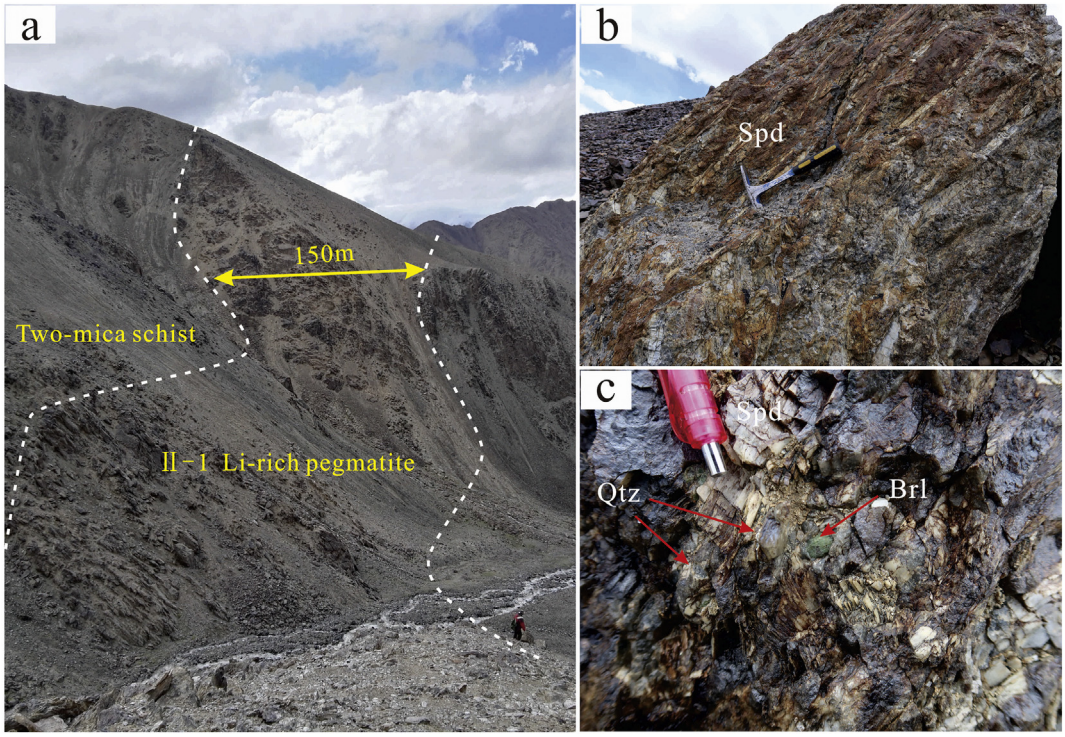

Fig. 4. Photographs showing the mineralization within the Bailongshan rare-metal deposit. Spd spodumene; Qtz quartz; Brl beryl.

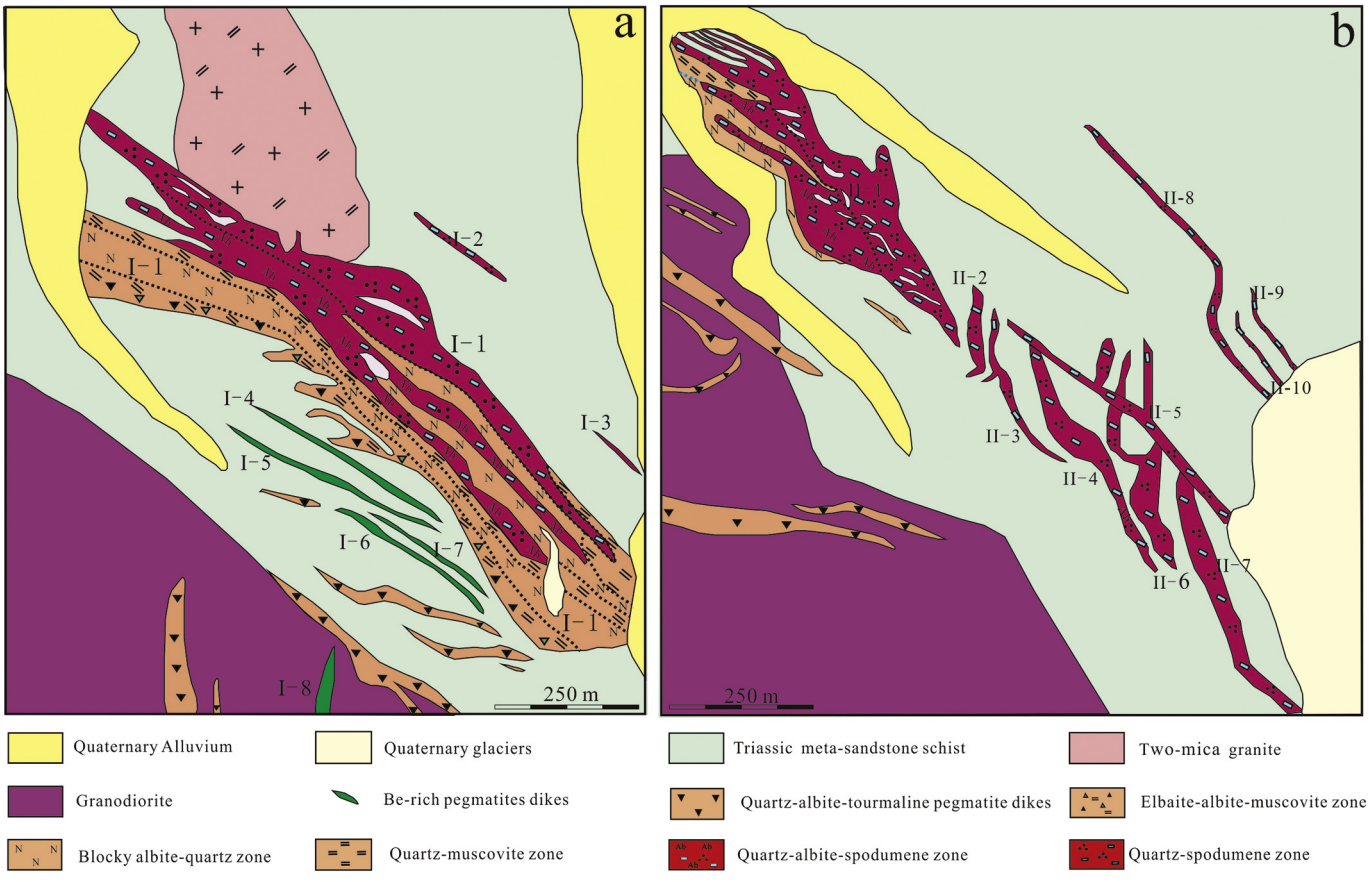

Fig. 5. Schematic geological map of mining segments I–II of the Bailongshan Li—Rb deposit showing regional and internal zonation.

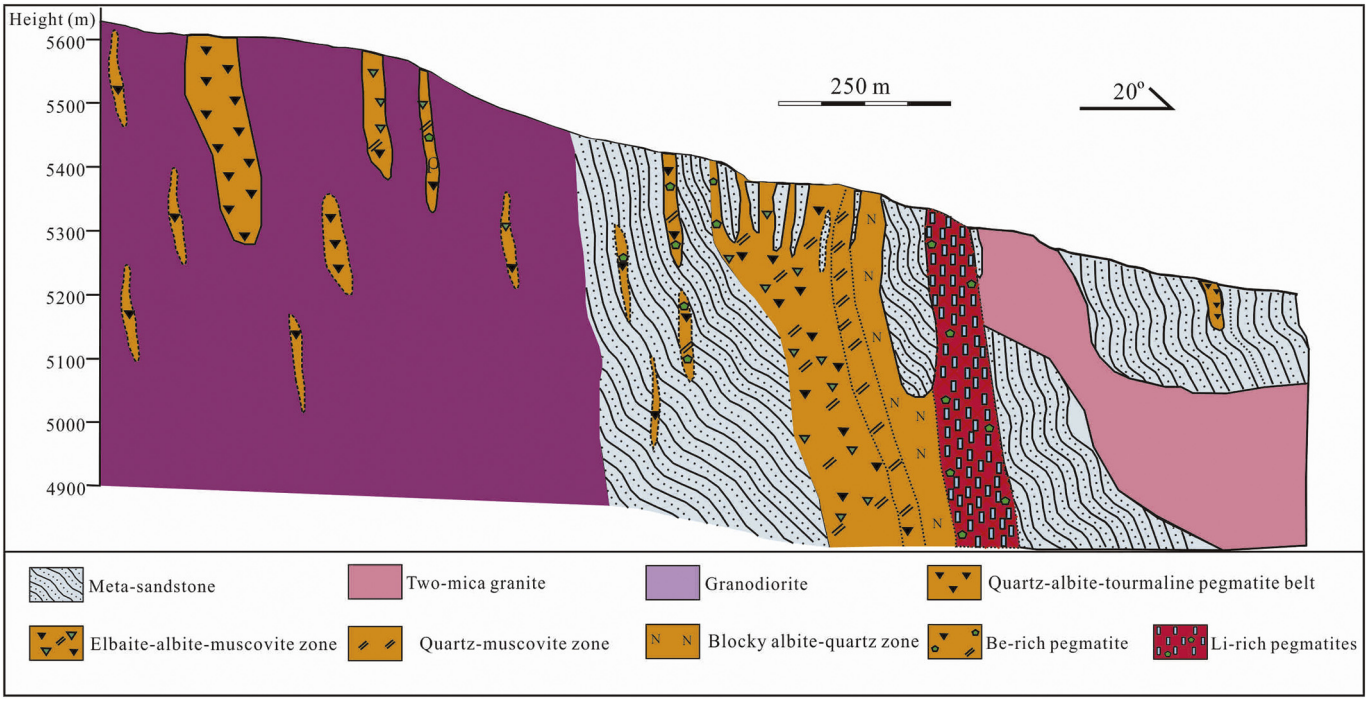

Fig. 6. Cross-section showing regional zonation in Segment I.

correction involved the procedure of Andersen (2002), and results and associated age calculations are shown in a concordia diagram (Fig. 7b) constructed using ISOPLOT (V.3.0; Ludwig, 2003).

4.3. LA–ICP–MS coltan U—Pb dating

Coltan U—Pb dating was carried out using a GeoLas PLUS 193-nm excimer ArF laser-ablation system coupled to an Agilent 7500a quadrupole ICP–MS at the State Key Laboratory for Mineral Deposits Research, Nanjing University, Nanjing, China. The laser was set to a fluence of ~12 J cm^{-3}, with a spot size of 43 μm and a repetition rate of 4 Hz. Coltan 139 from Madagascar with recorded U—Pb ages of 505.4 ± 1.0 Ma (BGR, Hannover, Germany; ID–TIMS), 506.6 ± 2.4 Ma (ID–TIMS), and 506.2 ± 5.0 Ma (LA–ICP–MS; Goethe University Frankfurt, Germany) (Melcher et al., 2015) was used as external calibration standard. Coltan 139 has a homogenous U—Pb isotopic composition and has been shown to be a suitable external reference for in situ Coltan U—Pb dating (Che et al., 2015; Melcher et al., 2015, 2017; Yan et al., 2018). Trace elements were calibrated using NIST SRM 610 combined with internal standardization. The analytical dwell time was 15 ms for ^{204}Pb, ^{206}Pb, and ^{208}Pb; 30 ms for ^{207}Pb; 10 ms for ^{232}Th and ^{238}U; and 6 ms for other elements. Every six analyses were followed by two analyses of Coltan 139 and two analyses of SRM 610. Each analysis involved 20 s of background acquisition, 50 s sample data acquisition, and up to 20 s of gas-blank acquisition. Data reduction was performed using ICPMSDataCal (Liu et al., 2010), and Isoplot 3.23 (Ludwing, 2003) was used to calculate the U—Pb age.

5. Results

5.1. Zircon U—Pb age

Zircon grains from granodiorite sample BLS–b5 are generally euhedral, with lengths of 100–300 μm and aspect ratios of 2–3. Most zircon grains are light yellow in color, transparent to translucent, prismatic, and exhibit clear oscillatory zoning in CL images. They contain 59–216 ppm Th and 96–382 ppm U, with Th/U ratios of 0.50–0.92, indicating an igneous origin (Belousova et al., 2002; Rubatto and Gebauer, 2000). Twenty-three spots yield concordant apparent $^{206}Pb/^{238}U$ ages of 213.8 ± 3.7 Ma to 210.3 ± 3.1, with a weighted-mean $^{206}Pb/^{238}U$ age of 212.3 ± 1.6 Ma (1σ; MSWD = 0.1; n = 18; Fig. 9a; Table 2).

5.2. Coltan U—Pb age

The coltan grains are generally tabular, 200–430 μm long, and 180–300 μm wide (Fig. 8c, d). They contain 1.08–11.67 ppm Th and 447–3248 ppm U. Twenty-four coltan grains were analyzed with concordant or near-concordant results, yielding a weighted-mean $^{206}Pb/^{238}U$ age of 208.1 ± 1.5 Ma (1σ; MSWD = 0.31; n = 2; Fig. 9b; Table 3). (See Table 4.)

6. Discussion

6.1. Age of the Bailongshan rare-metal deposit

Coltan-group minerals are common in rare-metal pegmatite deposits (e.g., Černý and Lenton, 1995; Selway et al., 2005). Coltan U—Pb ages provide direct constraints on the formation ages of coltan-bearing granites and pegmatites (e.g., Che et al., 2015; Romer et al., 1996; Romer and Wright, 1992; Yan et al., 2018). As coltan in the Bailongshan deposit is magmatic in origin, the coltan U—Pb age (208.1 ± 1.5 Ma) represents the crystallization age of the Bailongshan Li–Rb–(Be) rare-metal pegmatites. This age is similar to the granodiorite zircon U—Pb age (212.3 ± 1.6 Ma), indicating that both the granodiorite batholith and pegmatites crystallized in the Late Triassic, and may have a close genetic link.

There are >7000 pegmatites in the Dahongliutan–Bailongshan region (Yan et al., 2018). Columbite and cassiterite in the Dahongliutan deposit yielded pegmatite U—Pb emplacement ages of 211.9 ± 2.4 Ma and 218 ± 12 Ma, respectively (Yan et al., 2018), very similar to the age of the pegmatites in the Bailongshan deposit, indicating that the pegmatites in the Bailongshan–Dahongliutan region were also formed mainly in the Late Triassic, almost coeval with Middle Triassic–Early Jurassic magmatic rocks distributed widely along the West Kunlun orogenic belt.

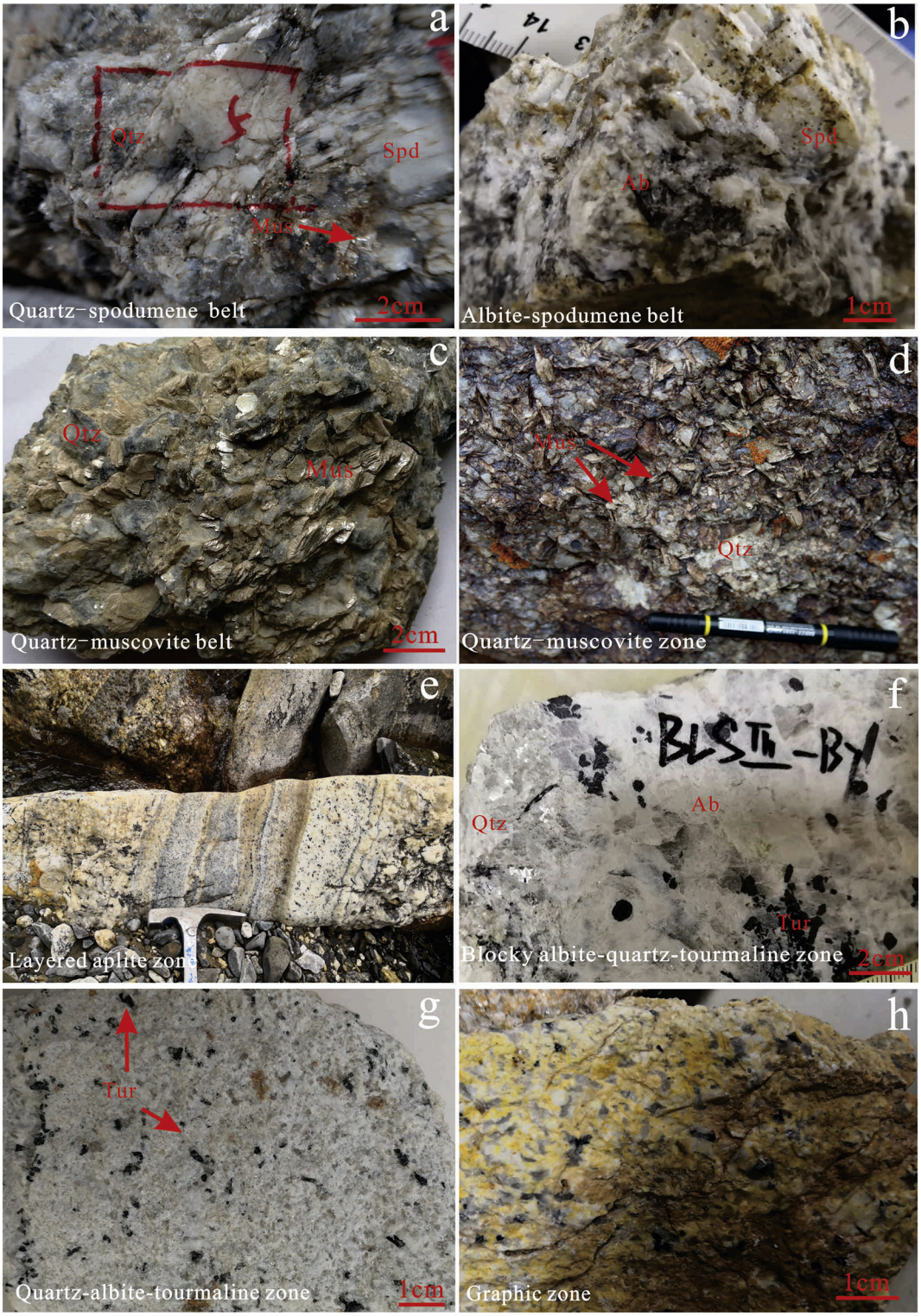

Fig. 7. Photographs of the various types of pegmatites found in the Bailongshan deposit. (a) Quartz–spodumene belt; (b) albite–quartz–spodumene belt; (c) quartz–muscovite belt; (d) quartz–muscovite zone; (e) layered aplite zone; (f) blocky albite–quartz–tourmaline zone; (g) quartz–albite–tourmaline zone; and (h) graphic zone. Spd spodumene; Ab albite; Mus muscovite; Tur tourmaline; Qtz quartz; Brl beryl.

6.2. Relationship between the pegmatites and granitoids

The Dahongliutan rare-metal pegmatites are genetically associated with the Triassic Dahongliutan S-type granitic pluton (Yan et al., 2018), and those in the Bailongshan region are distributed around a granodiorite batholith. The regional zonation of the pegmatites is symmetrical around the granodiorite and two-mica granite (Fig. 2), similar to the classical model of a zoned LCT-type pegmatite field (Černý, 1989). This indicates that the Bailongshan pegmatites may have evolved from highly fractionated granitic magma of the granodiorite batholith. The muscovite granite and two-mica granite plutons may also have evolved from granodioritic magmas, before eventually

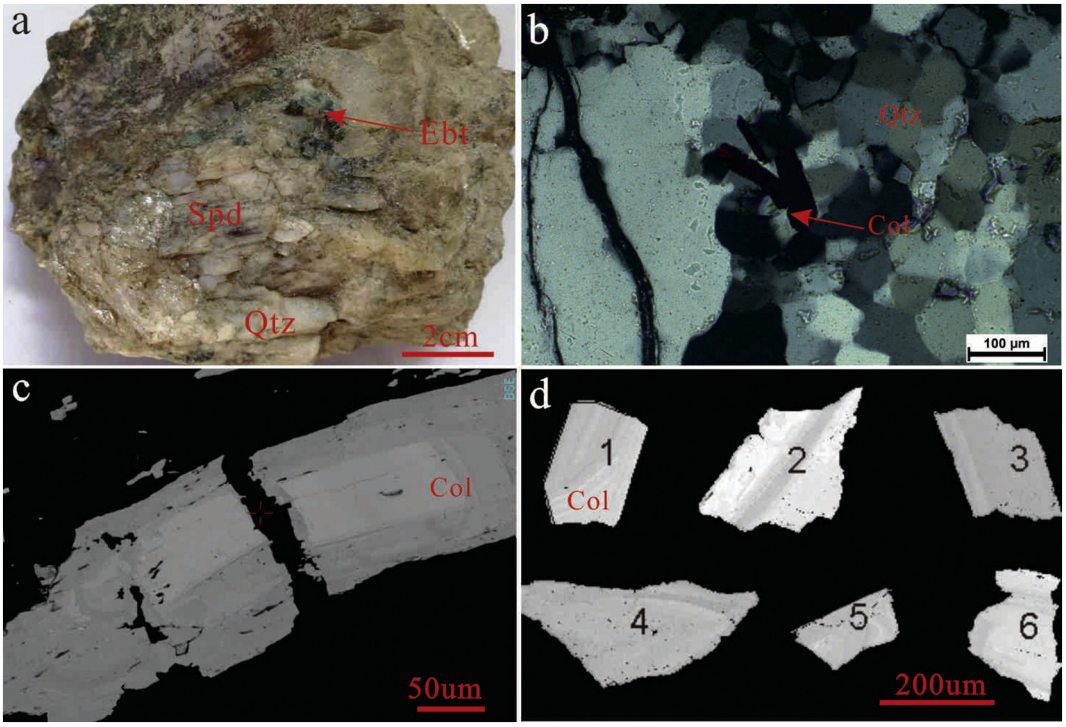

Fig. 8. The compositional and textural features of coltan from No. V–1 pegmatite. (a) The sample used for coltan U—Pb dating. (b) Photomicrograph showing the intergrowth of coltan, quartz, and spodumene. (c, d) BSE images showing the textural features of coltan. Qtz quartz; Ebt elbaite; Col coltan; Spd spodumene.

fractionating to pegmatitic melt. As a consequence, the pegmatites show great petrographic diversity, from biotite granite at depth through two-mica and muscovite + garnet facies, to caps of pegmatitic leucogranites. The significant difference in Li contents between the Li-poor and Li-rich pegmatites would have been caused by fractional crystallization of the granitic or pegmatitic melt.

Previous studies have shown that pegmatites may begin as a supercritical fluid, and magma fractionation during this supercritical stage could cause the observed variation in chemical compositions (Thomas and Davidson, 2016). Fractionation leads to progressive enrichment of incompatible ore-forming elements and volatile components (e.g., Li, Rb, Be, Cs, P, Cl, and F) in the residual fluid or melt (Thomas 2000, 2016; Mulja and Williams-Jones, 2018). High-volatility contents can reduce melt viscosity and liquidus temperature (Baker and Vaillancourt, 1995; Xiong et al., 1998), further delaying crystallization of the evolved magmas and providing an explanation for the regional zonation of the Bailongshan deposit (Mulja and Williams-Jones, 2018).

6.3. Late Triassic West Kunlun–Songpan–Garzê Li–Rb–(Be) rare-metal belt

The formation of the Bailongshan rare-metal pegmatite deposit is likely related to the tectonic evolution of the Paleo-Tethys Ocean and

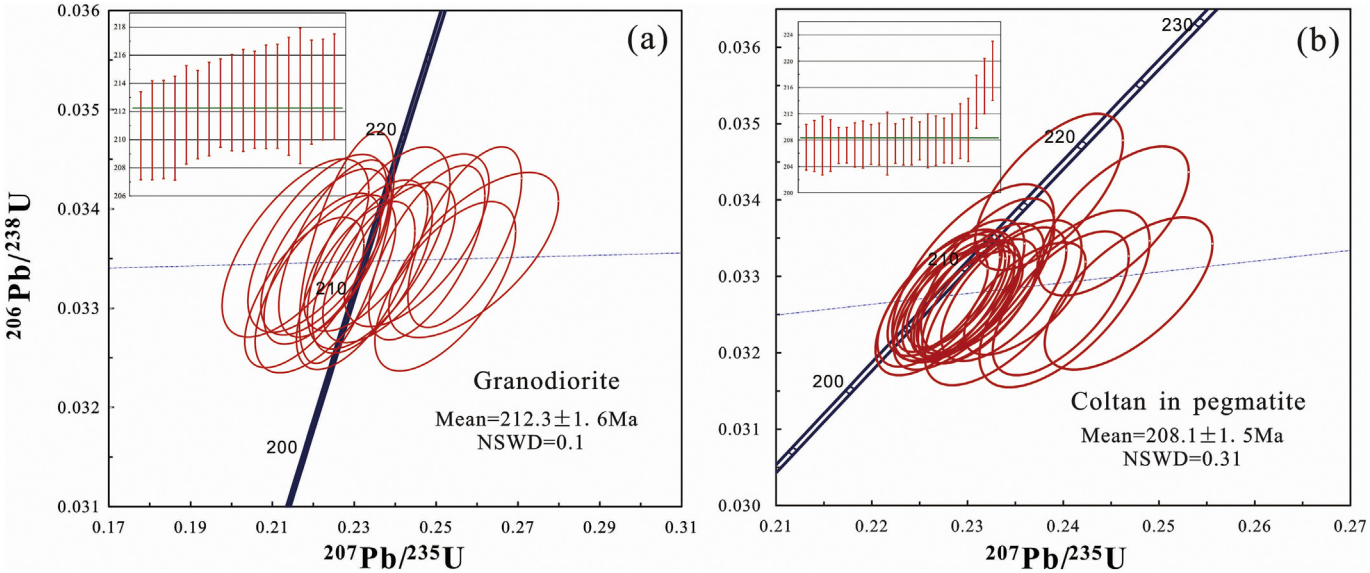

Fig. 9. U—Pb concordia diagrams and weighted-mean age calculations for (a) zircon from the Bailongshan granodiorite, and (b) coltan from the Bailongshan pegmatites.

Table 2
U—Pb for Zircon ages from the Bailongshan granodiorite batholith.

Spot no.	Concentration (ppm)		Ratio	Isotopic Ratio						Age/Ma			
	Th	U	Th/U	$^{207}Pb/^{206}Pb$	1σ	$^{207}Pb/^{235}U$	1σ	$^{206}Pb/^{238}U$	1σ	$^{207}Pb/^{235}U$	1σ	$^{206}Pb/^{238}U$	1σ
BLS-b5–1	63	109	0.58	0.0512	0.0026	0.2360	0.0115	0.0336	0.0007	215.1	9.5	213.1	4.2
BLS-b5–2	72	115	0.63	0.0487	0.0023	0.2228	0.0103	0.0336	0.0006	204.3	8.6	212.8	3.4
BLS-b5–3	88	144	0.61	0.0506	0.0023	0.2385	0.0107	0.0335	0.0005	217.2	8.8	212.2	3.3
BLS-b5–4	216	382	0.57	0.0467	0.0017	0.2282	0.0076	0.0336	0.0008	208.7	6.3	213.1	4.8
BLS-b5–5	109	188	0.58	0.0543	0.0023	0.2477	0.0094	0.0336	0.0006	224.7	7.6	212.8	3.6
BLS-b5–6	72	109	0.66	0.0471	0.0026	0.2156	0.0118	0.0336	0.0006	198.3	9.9	213.1	3.7
BLS-b5–7	126	253	0.50	0.0545	0.0026	0.2570	0.0092	0.0337	0.0006	232.2	7.4	213.8	3.7
BLS-b5–8	88	177	0.50	0.0509	0.0022	0.2329	0.0100	0.0335	0.0005	212.6	8.2	212.6	3.1
BLS-b5–9	73	125	0.58	0.0495	0.0021	0.2253	0.0091	0.0336	0.0006	206.3	7.5	213.0	3.7
BLS-b5–10	81	120	0.68	0.0506	0.0023	0.2344	0.0097	0.0334	0.0006	213.8	8.0	211.8	3.5
BLS-b5–11	115	169	0.69	0.0531	0.0025	0.2453	0.0117	0.0337	0.0006	222.7	9.5	213.6	3.6
BLS-b5–12	72	121	0.60	0.0470	0.0025	0.2210	0.0112	0.0337	0.0006	202.7	9.3	213.4	3.7
BLS-b5–13	79	130	0.60	0.0507	0.0021	0.2303	0.0096	0.0332	0.0006	210.5	7.9	210.7	3.5
BLS-b5–14	65	96	0.68	0.0572	0.0032	0.2592	0.0137	0.0335	0.0005	234.0	11.0	212.6	3.4
BLS-b5–15	59	99	0.60	0.0497	0.0026	0.2229	0.0113	0.0332	0.0006	204.4	9.4	210.8	3.7
BLS-b5–16	175	192	0.92	0.0471	0.0022	0.2178	0.0096	0.0332	0.0005	200.1	8.0	210.3	3.1
BLS-b5–17	66	100	0.65	0.0487	0.0021	0.2222	0.0094	0.0334	0.0005	203.7	7.8	211.8	3.1
BLS-b5–18	67	113	0.59	0.0557	0.0026	0.2522	0.0114	0.0332	0.0006	228.4	9.2	210.7	3.5

the Tianshuihai terrane (e.g., Pan, 1996; Matte et al., 1996; Mattern and Schneider, 2000; Xiao et al., 2005). Estimates of the timing of closure of the Paleo-Tethys Ocean and formation of the Mazar–Kangxiwar suture vary between the late Permian, Late Triassic, and Late Jurassic (Matte et al., 1996; Mattern and Schneider, 2000; Pan, 1996; Xiao et al., 2005). Many recent studies have shown that the Mazar–Kangxiwar suture formed earlier than 220 Ma (e.g., Wei et al., 2017; Yan et al., 2018), with the Bailongshan deposit thus forming in a post-collisional setting. Many large rare-metal pegmatite deposits formed in such a setting (Wang et al., 2005; Tkachev, 2011; Wang et al., 2007; Černý, 1991a, b). For example, most large rare-metal pegmatite deposits in the Chinese Altay formed in a post-collisional setting (Wang et al., 2005), and a global study of 140 LCT-type pegmatite deposits found that the emplacement of large rare-metal-bearing pegmatites occurred predominately in such settings (Tkachev, 2011).

The rare-metal pegmatite deposits in the West Kunlun orogenic belt are distributed around Late Triassic–Early Jurassic granitic plutons along the Mazar–Kangxiwar suture (Fig. 1), which is related to closure of the Paleo-Tethys Ocean during the Late Triassic (Yan et al., 2018). This suggests that Late Triassic granitic plutons could be a potential indicator for rare-metal mineralization along the West Kunlun orogenic belt. This systematic regional zonation of pegmatites in the Bailongshan region may be useful in future prospecting elsewhere in the belt.

The West Sichuan Li belt in the Songpan–Garzê belt hosts the Jiajika super-large deposit (reserves of 3.5 Mt. Li_2O), as well as the Ke'eryin large deposit and four medium-sized deposits, and is considered the largest Li metallogenic belt in China (Li et al., 2015). The Songpan–Garzê belt has a complex tectonic history resulting from the interaction between three major continental blocks (the North China, Yangtze, and Qiangtang–Changdu blocks) during closure of the Paleo-Tethys Ocean

Table 3
U—Pb age for Coltan from the V-1 Li-rich pegmatite in the Bailongshan deposit.

Spot no.	Concentration (ppm)	U	Isotopic Ratio						Age/Ma			
	Th		$^{207}Pb/^{206}Pb$	1σ	$^{207}Pb/^{235}U$	1σ	$^{206}Pb/^{238}U$	1σ	$^{207}Pb/^{235}U$	1σ	$^{206}Pb/^{238}U$	1σ
V-1-1	1.77	764	0.0507	0.0005	0.2385	0.0051	0.0341	0.0007	217.2	4.2	216.2	4.2
V-1-2	1.93	831	0.0509	0.0005	0.2289	0.0044	0.0326	0.0006	209.3	3.6	206.9	3.5
V-1-3	2.21	795	0.0528	0.0006	0.2452	0.0052	0.0337	0.0006	222.7	4.2	213.8	4.0
V-1-4	2.16	953	0.0513	0.0004	0.2313	0.0040	0.0327	0.0005	211.3	3.3	207.3	3.4
V-1-5	1.50	656	0.0519	0.0004	0.2473	0.0056	0.0345	0.0007	224.4	4.5	218.5	4.5
V-1-6	5.55	1431	0.0504	0.0003	0.2273	0.0031	0.0327	0.0004	208.0	2.6	207.2	2.7
V-1-7	5.10	777	0.0518	0.0004	0.2337	0.0054	0.0327	0.0007	213.3	4.5	207.2	4.5
V-1-8	2.84	712	0.0504	0.0004	0.2274	0.0046	0.0327	0.0006	208.0	3.8	207.2	3.9
V-1-9	1.63	522	0.0505	0.0005	0.2286	0.0042	0.0327	0.0006	209.0	3.5	207.7	3.5
V-1-10	2.70	771	0.0502	0.0005	0.2276	0.0039	0.0328	0.0005	208.2	3.3	207.9	3.4
V-1-11	1.27	545	0.0533	0.0005	0.2397	0.0047	0.0326	0.0006	218.2	3.8	207.1	3.9
V-1-12	3.99	1391	0.0506	0.0004	0.2296	0.0042	0.0328	0.0006	209.8	3.5	208.2	3.8
V-1-13	1.47	541	0.0511	0.0005	0.2321	0.0046	0.0330	0.0007	211.9	3.8	209.4	4.2
V-1-14	2.26	849	0.0519	0.0006	0.2338	0.0043	0.0328	0.0006	213.3	3.6	207.8	3.6
V-1-15	1.08	447	0.0532	0.0005	0.2401	0.0059	0.0327	0.0008	218.5	4.8	207.5	4.8
V-1-16	3.59	1244	0.0508	0.0004	0.2295	0.0036	0.0327	0.0005	209.8	3.0	207.3	3.0
V-1-17	3.84	1379	0.0512	0.0006	0.2302	0.0037	0.0327	0.0004	210.4	3.0	207.2	2.8
V-1-18	1.48	587	0.0544	0.0006	0.2468	0.0058	0.0328	0.0007	224.0	4.7	207.9	4.1
V-1-19	3.39	1237	0.0507	0.0005	0.2306	0.0056	0.0330	0.0008	210.7	4.6	209.6	4.8
V-1-20	5.18	1723	0.0512	0.0003	0.2314	0.0043	0.0328	0.0006	211.4	3.6	207.9	3.8
V-1-21	1.86	579	0.0511	0.0005	0.2299	0.0036	0.0327	0.0005	210.1	3.0	207.4	3.2
V-1-22	3.00	1125	0.0507	0.0004	0.2288	0.0034	0.0328	0.0005	209.2	2.8	207.9	2.9
V-1-23	7.15	2179	0.0521	0.0004	0.2360	0.0042	0.0327	0.0005	215.1	3.4	207.5	3.0
V-1-24	11.67	3248	0.0503	0.0004	0.2270	0.0042	0.0327	0.0006	207.7	3.5	207.3	3.6

Table 4
Available age data set for the rare-mental pegmatites and associated granitoids in the West Kunlun–Songpan-Ganzê rare-metal pegmatite metallogenic belt.

Ore field	Lithology	Methods	Age (Ma)	References
Jiajika	Two-mica granite	Zircon U-Pb	223 ± 1	Hao et al., 2015
	Pegmatite	Coltan U-Pb	214 ± 2	
Xuebaoding	Granodiorite	Zircon U-Pb	200.6 ± 1.3	Zhang et al., 2014b
	monzonite	Zircon U-Pb	193.7 ± 1.1	
	Pegmatite	Muscovite Ar-Ar	194.5 ± 1.0	
Dahongliutan	Two-mica granite	Zircon U-Pb	220 ± 2	Qiao et al., 2015
			217 ± 2	
	Pegmatite	Coltan U-Pb	211.9 ± 2.4	Yan et al., 2018
	Pegmatite	Cassiterite U-Pb	218 ± 12	
Zhawulong	Muscovite granite	Zircon U-Pb	211.6 ± 5.2	Li et al., 2019
	Pegmatite	Coltan U-Pb	204.5 ± 1.8	
Ke'eryin	Two-mica granite	Zircon U-Pb	207 ± 1205 ± 4	Zhang et al., 2014a; Yue et al., 2018
	Pegmatite	Zircon U-Pb	198 ± 3	Fei et al., 2018
Bailongshan	Granodiorite	Zircon U-Pb	212.3 ± 1.6	This study
	Pegmatite	Coltan U-Pb	208.1 ± 1.5	

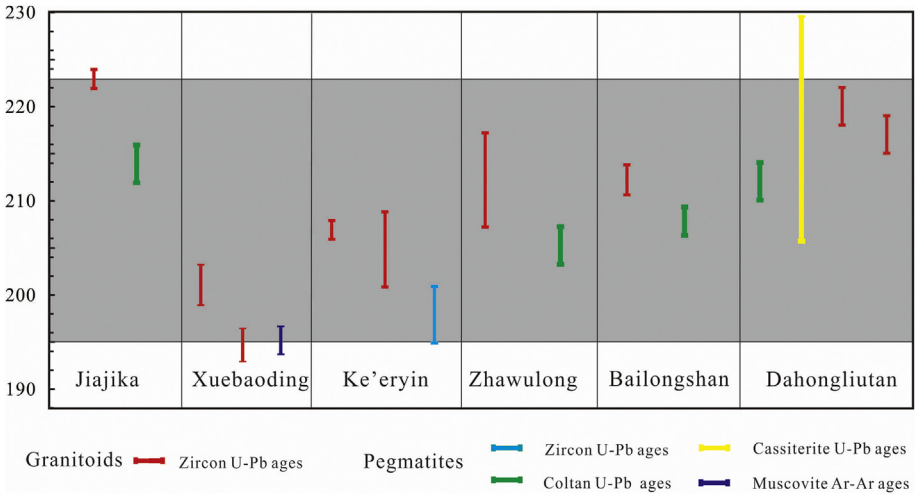

Fig. 10. Compilation of geochronological data from rare-metal pegmatite systems and granitic intrusions in the West Kunlun–Songpan–Garzê metallogenic belt (Li et al., 2019; Zhang et al., 2006; Zhang et al., 2014; Yan et al., 2018; Hao et al., 2015; Zhao et al., 2019; Qiao et al., 2015; Yue et al., 2018; Fei et al., 2018).

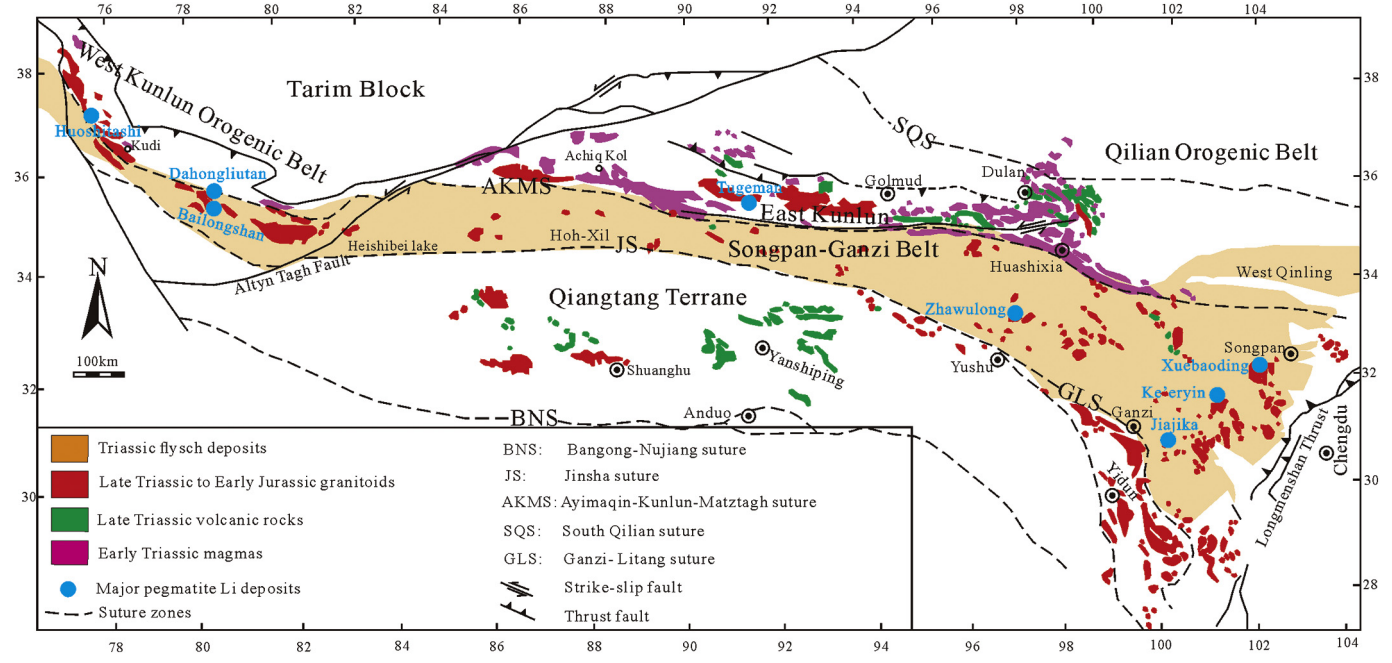

Fig. 11. Simplified tectonic map of the major Late Triassic igneous rocks and pegmatitic Li deposits of the Tibetan Plateau, Songpan–Garzê, West Kunlun, East Kunlun and other major terranes. Modified after Zhang et al. (2014) and Yin and Harrison (2000), with zircon U—Pb ages of the Late Triassic–Early Jurassic magmatic rocks from Zhang et al. (2014) and references therein.

(Roger et al., 2004; Harrowfield and Wilson, 2005), which led to the formation of a number of granitic pegmatite-type rare-metal deposits during the Late Triassic (Li et al., 2015; Xu et al., 2018).

Both the West Sichuan Li belt and the West Kunlun rare-metal belt were associated with the closure of the Paleo-Tethys Ocean in the Late Triassic. The Jiajika pegmatites were dated at ca. 200 Ma, with a muscovite Ar—Ar age of 199.4 ± 2.3 Ma (Li et al., 2015) and a coltan U—Pb age of 214 ± 2 Ma (Li et al., 2019; Table 4). The Xuebaoding pegmatites have a muscovite Ar—Ar age of 195 ± 1 Ma (Zhang et al., 2014b), and the Ke'eryin pegmatites have a zircon U—Pb age of 198 ± 3 Ma (Fei et al., 2018). These ages are slightly younger than those of the rare-metal pegmatites in the West Kunlun orogenic belt, but are still within the post-orogenic stage. Pegmatites in the West Sichuan metallogenic belt also have a close genetic relationship with Triassic granitoids: the Jiajika deposit occurs around a two-mica granite pluton with a zircon U—Pb age of 223 ± 1 Ma (Hao et al., 2015); and 548 mineralized pegmatite dikes in the Ke'eryin deposit are distributed in clusters around a 207 ± 1 Ma granitic complex (Fig. 10; Zhao et al., 2019). The Tianshuihai terrane may represent the westward extension of the Songpan–Garzê belt (Molnar et al., 1987; Matte et al., 1996; Pan, 1996; Mattern and Schneider, 2000; Xiao et al., 2003a). In that case, pegmatites in the West Kunlun rare-metal metallogenic belt may be genetically and geodynamically related to the Songpan–Garzê metallogenic belt, forming a >2000-km-long rare-metal belt running from West Kunlun, through East Kunlun, to West Sichuan: the West Kunlun–Songpan–Garzê rare-metal pegmatite metallogenic belt (Fig. 11). This tentative proposal is supported by the recent discovery of Zhawulong rare-metal pegmatites in the middle of this long metallogenic belt (Fig. 11), which has reserves of >160,000 t Li_2O, and also occurs around a muscovite granite pluton (212 ± 5 Ma; Li et al., 2019). The coltan U—Pb age of the pegmatites is 205 ± 2 Ma. An understanding of this giant metallogenic belt is important for future prospecting in southwest China.

7. Conclusions

The newly discovered Bailongshan rare-metal pegmatite deposit is a super-large Li–Rb–(Be–Ta–Nb) deposit in the West Kunlun orogenic belt. Fifty-two rare-metal orebodies have been recognized in the deposit, and ore reserves are estimated to be >5.06 million t Li_2O, 160,020 t BeO, 316,200 t Rb_2O, 40,060 t Nb_2O_5, and 10,750 t Ta_2O_5. The emplacement and mineralization of the Bailongshan pegmatites occurred at ca. 208 Ma, and they are temporospatially related to a granodiorite batholith (ca. 212 Ma). The pegmatite deposits make up a >600-km-long rare-metal belt in the West Kunlun orogenic belt. Late Triassic granitic plutons could be a potential exploration indicator for rare-metal mineralization in the belt. A >2000-km-long rare-metal metallogenic belt is tentatively outlined, running from West Kunlun, through East Kunlun to West Sichuan, making up the West Kunlun–Songpan–Garzê rare-metal belt.

Declaration of Competing Interest

None.

Acknowledgments

This study was financially supported by the Xinjiang Major Science and Technology project no. 2018A03004, National Natural Science Foundation of China (No: 41972088 and 91962215), China Postdoctoral Science Foundation (2019M663138), the Second Comprehensive Scientific Survey of the Qinghai–Tibet Plateau (2019QZKK0803), State Technology Support Program projects 2011BAB06B05 and 2015BAB05B03, and GIGCAS 135 project 135TP201601. Discussions with Christina Yan Wang, Qiang Wang, and Bin He significantly improved the original manuscript. We are grateful to Huaqin Zhang for assistance with the solution analyses and Huan Hu for assistance with the Coltan U—Pb age analyses.

References

Andersen, T., 2002. Correction of common lead in U–Pb analyses that do not report Pb. Chem. Geol. 192, 59–79.
Baker, D.R., Vaillancourt, J., 1995. The low viscosities of F+H2O-bearing granitic melts and implications for melt extraction and transport. Earth Planet. Sci. Lett. 132, 199–211.
Belousova, E.A., Griffin, W.L., O'Reilly, S.Y., Fisher, N.I., 2002. Igneous zircon: trace element composition as an indicator of source rock type. Contrib. Mineral. Petrol. 14 (5), 602–622.
Black, L.P., Kamo, S.L., Allen, C.M., Aleinikoff, J.N., Davis, D.W., Korsch, R.J., Foudoulis, C., 2003. TEMORA 1: a new zircon standard for Phanerozoic U–Pb geochronology. Chem. Geol. 200 (1), 155–170.
Černý, P., 1989. Exploration strategy and methods for pegmatite deposits of tantalum. In: Möller, P., Černý, P., Saupé, F. (Eds.), Lanthanides, Tantalum and Niobium. Springer-Verlag, Heidelberg, pp. 274–310.
Černý, P., 1991a. Fertile granites of Precambrian rare-element pegmatite fields: is geochemistry controlled by tectonic setting or source lithologies. Precambrian Res. 51, 429–468.
Černý, P., 1991b. Rare-element granitic pegmatites. Part II: Regional to global environments and petrogenesis. Geosci. Canada 18 (2).
Černý, P., Erict, T.S., 2005. The classification of granitic pegmatites revisited. Can. Mineral. 43, 2005–2026.
Černý, P., Lenton, P.G., 1995. The Buck and Pegli lithium deposits, southeastern Manitoba: the problem of updip fractionation in subhorizontal pegmatite sheets. Econ. Geol. 90, 658–675.
Che, X.D., Wu, F.Y., Wang, R.C., Gerdes, Axel, Ji, W.Q., Zhao, Z.H., Yang, J.H., Zhu, Z.Y., 2015. In situ U-Pb isotopic dating of columbite–tantalite by LA–ICP–MS. Ore Geol. Rev. 665, 978–989.
Deng, W.M., 1995. The geologic characteristics of the ophiolites in the Karakoram-West Kunlun region and their tectonic significance. Acta Petrol. Sin. 11 (suppl), 98–111.
Ding, D.G., Wang, D.X., Liu, W.X., 1996. The Western Kunlun Orogenic Belt and Basin (In Chinese). Geol. Publ. House Beijing 36, 1–224.
Fei, G., Tian, J., Yang, J., Gao, J., Tang, W., Li, J., Gu, C., 2018. New Zircon U-Pb Age of the Super-large Lijiagou Spodumene Deposit in Songpan Garzê Fold Belt, Eastern Tibet: Implications for early Jurassic Rare-Metal Polymetallic Event. Acta Geol. Sin. Engl. Ed. 92 (3), 1274–1275.
Hao, X.F., Fu, X.F., Liang, B., Yuan, L.P., Pan, M., Tang, Y., 2015. Formation ages of granite and X03 pegmatite vein in Jiajika, western Sichuan, and their geological significance. Mineral. Depos. 34 (6), 1199–1208.
Harrowfield, M.J., Wilson, C.J., 2005. Indosinian deformation of the Songpan-Garzê fold belt, northeast Tibetan Plateau. J. Struct. Geol. 27 (1), 101–117.
Hu, J., Wang, H., Huang, C., Tong, L., Mu, S., Qiu, Z., 2016. Geological characteristics and age of the Dahongliutan Fe-ore deposit in the Western Kunlun orogenic belt, Xinjiang, northwestern China. J. Asian Earth Sci. 116, 1–25.
Li, H., Zhang, H., Ling, M.X., Wang, F.Y., Ding, X., Zhou, J.B., Yang, X.Y., Tu, X.L., Sun, W.D., 2011. Geochemical and zircon U-Pb study of the Huangmeijian A-type granite: implications for geological evolution of the lower Yangtze River belt. Int. Geol. Rev. 53, 499–525.
Li, J.K., Zou, T.R., Liu, X.F., Wang, D.H., Xin, D., 2015. The Metallogenetic Regularities of Lithium Deposits in China. Acta Geol. Sin. (Engl. Ed.) 89 (2), 652–670.
Li, P., Li, J., Chou, I., Wang, D., Xiong, X., 2019. Mineralization Epochs of granitic rare-metal pegmatite deposits in the Songpan–Garzê Orogenic belt and their implications for orogeny. Minerals 9 (5), 280.
Linnen, R.L., Cuney, M., 2005. Granite-related rare-element deposits and experimental constraints on Ta-Nb-W-Sn-Zr-Hf mineralization. In: Linnen, R.L., Samson, I.M. (Eds.), Rare-Element Geochemistry and Mineral Deposits. Geological Association of Canada, GAC (short course).
Liu, Y.S., Gao, S., Hu, Z.C., Gao, C.G., Zong, K.Q., Wang, D.B., 2010. Continental and oceanic crust recycling-induced melt–peridotite interactions in the Trans-North China Orogen: U–Pb dating, Hf isotopes and trace elements in zircons from mantle xenoliths. J. Petrol. 51, 537–571.
Ludwig, K.R., 2003. User's manual for isoplot/ex version 3.00—a geochronology toolkit for microsoft excel. Berk. Geochronol. Center Spec. Publ. 4, 1–70.
Matte, P., Tapponnier, P., Arnaud, N., Bourjot, L., Avouac, J.P., Vidal, P., Liu, Q., Pan, Y., Wang, Y., 1996. Tectonics of western Tibet, between the Tarim and the Indus. Earth Planet. Sci. Lett. 142, 311–330.
Mattern, F., Schneider, W., 2000. Suturing of the Proto- and Paleo-Tethys oceans in the Western Kunlun (Xinjiang, China). J. Asian Earth Sci. 18, 637–650.
Melcher, F., Graupner, T., Gäbler, H.E., Sitnikova, M., Henjes-Kunst, F., Oberthür, T., Gerdes, A., Dewaele, S., 2015. Tantalum-(niobium-tin) mineralisation in African pegmatites and rare metal granites: constraints from Ta-Nb oxide mineralogy, geochemistry and U-Pb geochronology. Ore Geol. Rev. 64, 667–719.
Melcher, F., Graupner, T., Gäbler, H.E., Sitnikova, M., Oberthür, T., Gerdes, A., Chudy, T., 2017. Mineralogical and chemical evolution of tantalum–(niobium–tin) mineralization in pegmatites and granites. Part 2: Worldwide examples (excluding Africa) and an overview of global metallogenetic patterns. Ore Geol. Rev. 89, 946–987.
Molnar, P., Burchfiel, B.C., Zhao, Z., Liang, K., Wang, S., Huang, M., 1987. Geologic evolution of northern Tibet: results of an expedition to Ulugh Muztagh. Science 235 (4786), 299–305.
Mulja, T., Williams-Jones, A.E., 2018. The physical and chemical evolution of fluids in rare-element granitic pegmatites associated with the Lacorne pluton, Québec, Canada. Chem. Geol. 493, 281–297.

Pan, Y.S., 1996. Geological Evolution of the Karakorum and Kunlun Mountains. Seismological Press, Beijing (In Chinese).

Peng, H.L., He, N.Q., Wang, M.C., Du, B., Li, W.J., Liu, Y.Q., 2018. Geological characteristics and Metallogenic regularity of West Track 509 rare polymetallic deposit in Dahongliutan region, Hetian, Xinjiang. Northwest. Geol. 51, 146–154 (in Chinese with English abstract).

Qiao, G.B., Zhang, H.D., Wu, Y.Z., Jin, M.S., Du, W., Zhao, X.J., Chen, D.H., 2015. Petrogenesis of the Dahongliutan Monzogranite in Western Kunlun: constraints from SHRIMP Zircon U-Pb geochronology and geochemical characteristics. Acta Geol. Sin. 89 (7), 1180–1194 (In Chinese).

Roger, F., Malavieille, J., Leloup, P.H., Calassou, S., Xu, Z., 2004. Timing of granite emplacement and cooling in the Songpan–Garzê Fold Belt (eastern Tibetan Plateau) with tectonic implications. J. Asian Earth Sci. 22 (5), 465–481.

Romer, R.L., Wright, J.E., 1992. U-Pb dating of columbites: a geochronologic tool to date magmatism and ore deposits. Geochim. Cosmochim. Acta 56, 2137–2142.

Romer, R.L., Smeds, S.A., Cenery, P., 1996. Crystal-chemical and genetic controls of U-Pb systematics of columbite–tantalite. Mineral. Petrol. 57, 243–260.

Rubatto, D., Gebauer, D., 2000. Use of cathodoluminescence for U–Pb zircon dating by ion microprobe: some examples from the Western Alps. Cathodoluminescence in Geosciences. Springer, Berlin Heidelberg, pp. 373–400.

Selway, J.B., Breaks, F.W., Tindle, A.J., 2005. A review of rare-element (Li-Cs-Ta) pegmatite exploration techniques for the Superior Province, Canada, and large worldwide tantalum deposits. Explor. Min. Geol. 14 (1), 1–30.

Thomas, R., Davidson, P., 2016. Revisiting complete miscibility between silicate melts and hydrous fluids, and the extreme enrichment of some elements in the supercritical state—Consequences for the formation of pegmatites and ore deposits. Ore Geol. Rev. 72, 1088–1101.

Tkachev, A.V., 2011. Evolution of metallogeny of granitic pegmatites associated with orogens throughout geological time. Geol. Soc. Lond. Spec. Publ. 350 (1), 7–23.

Wang, D.H., Li, J.K., Fu, X.F., 2005. $^{40}Ar/^{39}Ar$ dating for the Jiajika pegmatite-type rare metal deposit in western Sichuan and its significance. Geochimica 34, 541–547 (in Chinese with English abstract).

Wang, T., Tong, Y., Jahn, B.M., Zou, T.R., Wang, Y.B., Hong, D.W., Han, B.F., 2007. SHRIMP U \Pb Zircon geochronology of the Altai no. 3 Pegmatite, NW China, and its implications for the origin and tectonic setting of the pegmatite. Ore Geol. Rev. 32, 325–336.

Wang, H., Li, P., Ma, H.D., Zhu, B.Y., Qiu, L., Zhang, X.Y., Yan, Q.H., 2017. Discovery of the Bailongshan Super-large Lithium-Rubidium Deposit in Karakorum, Hetian, Xinjiang, and its prospecting implication. Geotecton. Metallog. 41 (6), 1053–1062.

Wang, H., Gao, H., Ma, H.D., Zhu, B.Y., Zhou, L., Zhu, X.Y., Wang, Q.H., Wang, H.D., Dong, B.Y., Yan, L., Zhang, X.Y., 2019. Preliminary study on geological characteristics and pegmatite vein group zoning of Xuefengling lithium deposit, Xuepen Lithium deposit, Shuangya lithium deposit in Karakorum, Hetian, Xinjiang. Geotectonica et Metallogenica https://doi.org/10.16539/j.ddgzyckx.2020.01.005.

Wei, X.P., Wang, H., Hu, J., Mu, S.L., Qiu, Z.W., Yan, Q.H., Li, P., 2017. Geochemistry and geochronology of the Dahongliutan two-mica granite pluton in western Kunlun orogen: Geotectonic implications. Geochimica 46 (1), 66–80.

Xiao, W.J., Windley, B.F., Chen, H.L., Zhang, G.C., Li, J.L., 2002a. Carboniferous-Triassic subduction and accretion in the western Kunlun, China: implications for the collisional and accretionary tectonics of the northern Tibetan plateau. Geology 30, 295–298.

Xiao, W.J., Han, F.L., Windley, B.F., Yuan, C., Zhou, H., Li, J.L., 2003a. Multiple accretionary orogenesis and episodic growth of continents: insights from the western Kunlun Range, Central Asia. Int. Geol. Rev. 45, 303–328.

Xiao, W.J., Windley, B.F., Hao, J., Zhai, M.G., 2003b. Accretion leading to collision and the Permian Solonker suture, Inner Mongolia, China: termination of the central Asian orogenic belt. Tectonics 22, 1069. https://doi.org/10.1029/2002TC001484.

Xiao, W.J., Windley, B.F., Liu, D.Y., Jian, P., Liu, C.Z., Yuan, C., Sun, M., 2005. Accretionary tectonics of the Western Kunlun orogen, China: a Paleozoic-early Mesozoic, long lived active continental margin with implications for the growth of southern Eurasia. J. Geol. 113, 687–705.

Xiong, X.L., Zhao, Z.H., Zhu, J.C., Rao, B., Lai, M., 1998. Experiments on the fluid/melt partition of fluorine in the system albite graniteH2O-HF. Geochimica 27, 67–73.

Xu, Z., Wang, R., Zhao, Z., Fu, X., 2018. On the structural back grounds of the large-scale "hard-rock type" lithium ore belts in China. Acta Geol. Sin. 92, 1091–1106.

Yan, Q.H., Qiu, Z.W., Wang, H., Wang, M., Wei, X.P., Li, P., Liu, J.P., 2018. Age of the Dahongliutan rare metal pegmatite deposit, West Kunlun, Xinjiang (NW China): Constraints from LA–ICP–MS U–Pb dating of columbite-(Fe) and cassiterite. Ore Geol. Rev. 100, 561–573.

Yang, Zhanshan, Yanhua, Li, Ye, Haitao, 2012. Research on process control of producing carnallite in salt pan. Ind. Miner. Process. 41 (4), 15–16 (in Chinese).

Yin, J.X., Bian, Q.T., 1995. Geological Map of the Karakoram-West Kunlun and Adjacent Regions. Science Press, Beijing.

Yin, A., Harrison, T.M., 2000. Geologic evolution of the Himalayan-Tibetan orogen. Annu. Rev. Earth Planet. Sci. 28 (1), 211–280.

Yue, X., Guo, J., Mao, S., Zhu, Z., Tan, H., 2018. Zircon U–Pb age and geochemistry of the Taiyanghe granitoid in western Sichuan, China and its geological significance. Bull. Mineral. Petrol. Geochem. 37, 1142–1151.

Zhang, H.F., Zhang, L., Harris, N., Jin, L.L., Yuan, H., 2006. U–Pb zircon ages, geochemical and isotopic compositions of granitoids in Songpan–Garzê fold belt, eastern Tibetan Plateau: constraints on petrogenesis and tectonic evolution of the basement. Contrib. Mineral. Petrol. 152 (1), 75–88.

Zhang, L.Y., Ding, L., Pullen, A., Xu, Q., Liu, D.L., Cai, F.L., Kapp, P., 2014a. Age and geochemistry of western Hoh-Xil–Songpan-Ganzi granitoids, northern Tibet: Implications for the Mesozoic closure of the Paleo-Tethys Ocean. Lithos 190, 328–348.

Zhang, D., Peng, J., Coulson, I.M., Hou, L., Li, S., 2014b. Cassiterite U–Pb and muscovite $^{40}Ar–^{39}Ar$ age constraints on the timing of mineralization in the Xuebaoding Sn–W–Be deposit, western China. Ore Geol. Rev. 62, 315–322.

Zhao, Z.B., Du, J.X., Liang, F.H., Wu, C., Liu, X.J., 2019. Structure and metamorphism of Markam gneiss dome from the eastern Tibetan plateau and its implications for crustal thickening, metamorphism, and exhumation. Geochem. Geophys. Geosyst. 20 (1), 24–45.

Zhou, B., Sun, Y.X., Kong, D.Y., 2011. Geological features and prospecting potential of rare metallic deposits in the Dahongliutan region, Xinjiang. Acta Geol. Sichuan 31 (3), 288–292 (in Chinese with English abstract).